Effect of grain size distribution of sandy soil on the shearing behaviors at soil-structure interface

Han-Lin Wang, Ph.D., A.M.ASCE [1]; Wan-Huan Zhou, M.ASCE [2, *]; Zhen-Yu Yin [3]; Xi-Xi Jie [4]

[1] Post-doctoral Fellow, Department of Civil and Environmental Engineering, Faculty of Science and Technology, University of Macau, Macau, China. ORCID: https://orcid.org/0000-0002-5416-9392. Email: wanghanlin@zju.edu.cn

[2] Associate Professor, Department of Civil and Environmental Engineering, Faculty of Science and Technology, University of Macau, Macau, China; Associate Professor, Zhuhai UM Science & Technology Research Institute (ZUMRI), Zhuhai, China (corresponding author). ORCID: http://orcid.org/0000-0001-5183-9947. Email: hannahzhou@umac.mo

[3] Associate Professor, Department of Civil and Environmental Engineering, The Hong Kong Polytechnic University, Kowloon, Hong Kong, China. Email: zhenyu.yin@polyu.edu.hk

[4] Former MSc student, Department of Civil and Environmental Engineering, Faculty of Science and Technology, University of Macau, Macau, China. Email: mb45496@connect.umac.mo

* Corresponding author

Abstract: For the geotechnical construction and maintenance, assessing the shearing behavior at the soil-structure interface is significant. This study presents an experimental investigation about the effect of the grain size distribution of a sandy soil on the shearing behaviors at the soil-structure interface, using a modified direct shear apparatus. Five soil samples with different coefficients of uniformity were prepared. The normalized roughness of the structure surface (the ratio between the maximum roughness of the structure plate and the mean grain size of the soil), the relative density, the maximum, the mean and the minimum grain sizes of all samples were controlled the same. During the tests, the shear force, the shear displacement and the vertical displacement were monitored. The results show that at a given shear displacement and normal stress, the sample with lower coefficient of uniformity C_u presents higher shear stress and more pronounced dilative behavior. The increase of C_u leads to the decrease of the friction angle for the soil-structure interface (at both peak and ultimate states) and the decrease of the maximum vertical deformation of the soil sample during the shearing process. As C_u increases, the main force chain at the soil-structure interface turns from the contact between the coarser grains to that mainly formed by the finer grains, resulting in the decrease of the shearing resistance. In comparison with the previous relevant studies, the decreasing trend of the friction angle with the increase of C_u is strongly supported.

Keywords: soil-structure interface, grain size distribution, coefficient of uniformity, friction angle, dilatancy

Introduction

In the field of geotechnical and geological engineering contents such as piled foundations, geosynthetic-reinforced structures, soil nailing projects and retaining walls, the soil-structure interaction plays a key role in the long-term performance of these constructed facilities (Abu-Farsakh et al. 2007; Zhou and Yin 2008; Yin and Zhou 2009; Zhou et al. 2011; Anubhav and Basudhar 2013; Chen et al. 2013; Qian et al. 2013; Zhou et al. 2013; Arulrajah et al. 2014; Divya et al. 2014; Venkateswarlu et al. 2018; Wang et al. 2018a; Goodarzi and Shahnazari 2019; Wang and Chen 2019; Wang et al. 2019a, 2019b, 2019c). Among the mechanical behaviors for the soil-structure interface, assessing the shearing behavior is of paramount importance, which thus attracts increasing attentions from researchers in the recent decades.

The shearing behavior at the soil-structure interface is complex, with various influencing factors. Among these factors, the surface roughness of the structure was widely studied and was proven to significantly affect the shearing behaviors at the soil-structure interface (Uesugi and Kishida 1986; Jensen et al. 1999; Dove and Jarrett 2002; Hu and Pu 2004; Zhang and Zhang 2006; DeJong and Westgate 2009; Hamid and Miller 2009; Chen et al. 2015; Jing et al. 2018; Su et al. 2018; Zhou et al. 2019). To standardize this effect, a normalized surface roughness R_n was proposed by Uesugi and Kishida (1986), defined as the ratio between the maximum roughness of the structure plate $R_{\max}$ and the mean grain size d_{50} of the soil. As R_n increased in the beginning, the friction coefficient increased; when R_n reached a critical value, the friction coefficient stabilized irrespective of the variation of R_n (Uesugi and Kishida 1986; Jing et al.

66 2018; Su et al. 2018). Except for the surface roughness of the structure, other influential
67 factors such as loading conditions and soil properties on the shearing behaviors at the
68 soil-structure interface were also reported by several studies using numerical and
69 experimental methods (Desai et al. 1985; Uesugi and Kishida 1986; Zeghal and Edil
70 2002; Oumarou and Evgin 2005; Zhang and Zhang 2006; Mortara et al. 2007; DeJong
71 and Westgate 2009; Hamid and Miller 2009; Tabatabaiefar et al. 2013; Turan et al. 2013;
72 Hokmabadi et al. 2014; Trombetta et al. 2014; Eid et al. 2015; Hokmabadi et al. 2015;
73 Karimi and Dashti 2016; Nguyen et al. 2017; Fatahi et al. 2018; Jing et al. 2018; Su et
74 al. 2018; Zhu et al. 2018; Zhou et al. 2019). However, in terms of the soil properties,
75 the investigation about the influence of the grain size distribution of soils on the
76 shearing behavior at the soil-structure interface remains scarce.

77 In fact, as reported in literature, the grain size distribution of the soil has a
78 significant impact on the mechanical behaviors of the geotechnical materials (Kokusho
79 et al. 2004; Wichtmann and Triantafyllidis 2009; Yan and Dong 2011; Wang et al. 2013;
80 Wichtmann and Triantafyllidis 2013; Liu et al. 2014; Norsyahariati et al. 2016; Wang
81 et al. 2017, 2018b, 2018c). Based on this consideration, Uesugi and Kishida (1986)
82 conducted a series of shear tests to investigate the effect of the grain size distribution
83 of sandy soils on the shearing behaviors at the soil-structure interface. They stated that
84 the influence of the coefficient of uniformity C_u on the friction coefficient of the soil-
85 structure interface was insignificant. However, this conclusion was not rigorous, using
86 the samples with only two different coefficients of uniformity, different maximum /
87 minimum grain sizes, and an extremely low R_n value (about 0.006 and 0.03). This

value was much smaller than the critical R_n value ranging from 0.1 to 0.18 for this soil (Uesugi and Kishida 1986), suggesting that the variations of the friction coefficient had not reached the stable state and some estimating errors might thus be induced. Liang et al. (2017) investigated the shearing behavior of the soil-steel interface at various grain size distributions of a sand-stone mixture, with the same steel plate. Nevertheless, the mean grain sizes d_{50} were different for the samples, leading to the variations of the normalized surface roughness R_n. As a result, the different R_n values might also affect the testing results (Uesugi and Kishida 1986; Jing et al. 2018; Su et al. 2018; Zhou et al. 2019). Thereby, to the authors' knowledge, the effect of the grain size distribution of soils on the shearing behavior at the soil-structure interface has not been fully addressed yet.

In this study, a series of shear tests on the soil-structure interface were performed using a modified direct shear apparatus at five different grain size distributions for a sandy soil. The maximum, the mean and the minimum grain sizes, and the relative density of each sample were kept the same. One steel plate with the regular saw-tooth plate and a constant maximum surface roughness was used as the testing structure, which also indicates a constant R_n value. During the tests, the shear force, the horizontal shear displacement and the vertical displacement of the shear box were monitored. The testing results allow the effect of the grain size distribution of this sandy soil on the shearing behavior at the soil-structure interface to be analyzed.

Materials and Methods

Testing Materials

In this study, the Fujian standard sand was taken as the testing material. The soils were stored in sealed plastic bags in the laboratory with constant temperature and humidity. With three randomly selected soil samples, the water contents were determined by the oven-dry method as 0.059%, 0.073% and 0.090%, respectively, suggesting that this stored sandy soil can be approximately considered as dry sand with such low water content. In the following tests, the soils with this state of negligible water content were used.

In order to investigate the effect of the grain size distribution of soils on the soil-structure interface behaviors, the sandy soil was firstly sieved through different grain sizes between 0.212 mm and 2 mm, as shown by the photos of the sand particles (100 g mass for each photo) with different grain size ranges in Fig. 1. These particles have well-rounded corners and edges, determining the mean roundness parameter at about 0.88 by the particle projection and the image processing procedures [the roundness herein is defined as $(2\sqrt{\pi A})/P$ by Hentschel and Page (2003): π is the circular constant, A is the particle image projection area, P is the particle image projection perimeter; with the roundness value closer to 1, the particle shape is closer to a completely round one; see more details about the determination of the roundness of this sand in Li et al. (2018)]. Then, the sieved soils with different grain sizes and mass fractions were mixed to obtain soil samples with different grain size distribution curves, as shown in Fig. 2. In this study, five grain size distributions were considered, showing the variation of the coefficient of uniformity C_u ranging from 1.85 to 5.20. According

132 to ASTM (2017), the testing soils can be classified as poorly graded sand (SP). Table 1
133 lists the detailed soil properties. Note that to eliminate the extra influencing factors
134 except for C_u, the maximum, the minimum and the mean grain sizes were controlled
135 as the same. In addition, during the sample preparation, the relative densities of all
136 samples were kept at 90%.

137 ***Testing Apparatus and Methods***

138 The schematic view of the modified direct shear apparatus is shown in Fig. 3. The shear
139 box consists of two parts: the base fixed with the regular saw-tooth plate and the upper
140 part (sample size: 100 mm × 100 mm × 20 mm) filled with the soil sample (Fig. 3b).
141 For the saw-tooth plate, a constant maximum surface roughness $R_{\max}$ was provided.
142 According to the tests on the same kind of sand by Su et al. (2018), when the normalized
143 surface roughness R_n was higher than about 0.4, the friction angle of the soil-structure
144 interface remained relatively stable regardless of the change of R_n. Hence, in this study,
145 the R_n value was chosen as 0.8, to ensure that the stable values of the friction angle
146 could be obtained. Thus, the corresponding $R_{\max}$ value was back-calculated as 0.636
147 mm ($d_{50} = 0.795$ mm, see Table 1).

148 For the testing procedures, the selected saw-tooth plate ($R_{\max} = 0.636$ mm) and the
149 upper box were firstly installed to the base of the shear box. Secondly, the soil samples
150 with the pre-determined mass (calculated through the parameters in Table 1) were
151 prepared by leveling and compacting with a rubber hammer in three layers in the shear
152 box. After that, the sample was covered by the top plate and the shear box was installed
153 in the modified direct shear apparatus (Fig. 3a). Fourthly, the base of the shear box was

154 fixed to the shear apparatus and the bolts connecting the upper box and the base were
155 unscrewed. Then, the normal stress σ_n was applied through the loading system. In
156 this study, three normal stresses were considered for each sample: 50 kPa, 100 kPa and
157 200 kPa.

158 According to ASTM (2011) for the direct shear test, the default time for the poorly
159 graded sand [with less than 5% fines (particle size < 0.075 mm)] to failure was
160 recommended as 10 min. From the previous interface shear tests by Su et al. (2018) for
161 the same kind of sand with various roughness-value saw-tooth plates, the relative
162 displacement of 10 mm was found to be sufficient for the soil to enter the ultimate state.
163 Thus, the constant shear velocity of 1 mm/min (10 mm/10 min) was selected for the
164 present test, by driving the base with the saw-tooth plate horizontally and keeping the
165 upper box filled with the soil sample static. Finally, the tests terminated after the shear
166 displacement reached 12 mm, at which value the soil samples were expected to enter
167 the ultimate state (Su et al. 2018). During the tests, the shear force, the shear
168 displacement and the vertical displacement were monitored by the force sensor
169 (accuracy: 0.1 N), the horizontal and the vertical linear variable displacement
170 transformers (LVDT; accuracy: 0.001 mm), respectively (Fig. 3a).

171 Note also that to verify the testing accuracy of the proposed experiments before the
172 formal tests, three repeatability tests were performed on three samples of S1 (see
173 properties in Table 1 and Fig. 2) under 50 kPa normal stress.

174

175 **Experimental Results**

176 ***Repeatability Tests***

177 To check and to validate the accuracy of the testing methods, the repeatability tests
178 appear necessary. Fig. 4 shows the repeatability testing results about the variations of
179 the shear stress and the vertical displacement versus the shear displacement for three
180 S1 samples under 50 kPa normal stress. In the shear stress-shear displacement plane
181 (Fig. 4a), the peak and the ultimate shear stresses are defined as the maximum shear
182 stress during the shearing process and the shear stress at 12 mm shear displacement,
183 respectively. With regard to the relationship between the vertical displacement and the
184 shear displacement (Fig. 4b), dilatancy is considered for the positive vertical
185 displacement values and contraction is considered negative. The maximum vertical
186 displacement is defined as the maximum value of the positive vertical displacement
187 (dilatancy) during the shearing process. It can be observed from Fig. 4 that appropriate
188 repeatability can be obtained for both the shear stress and the vertical displacement
189 curves.

190 To quantify the repeatability of these tests, an uncertainty parameter is defined as
191 the ratio between the variation range of the value of a specific parameter (peak or
192 ultimate shear stress, maximum vertical displacement during shearing) and the average
193 value of this parameter for the three tests (Seif El Dine et al. 2010). With the lower
194 value of the uncertainty parameter, more accuracy can be obtained by the test. In terms
195 of the peak and the ultimate shear stresses, the uncertainty parameters are determined
196 as 1.55% and 2.87%, respectively. For the maximum vertical displacement, the
197 uncertainty parameter is calculated as 5.13%, which is slightly larger than those for the

198 specific shear stresses. Nevertheless, the relatively low values of the uncertainty
199 parameters still verify and ensure the repeatability by the present testing apparatus and
200 methods.

201 ***Stress-Displacement Curves***

202 Figs. 5-7 present the variations of the shear stress and the vertical displacement against
203 the shear displacement for each sample under 50 kPa, 100 kPa and 200 kPa normal
204 stresses, respectively. Note that the testing data of the sample with $C_u = 1.85$ (S1) under
205 50 kPa normal stress in Fig. 5 is represented by the repeatability Sample A in Fig. 4.
206 From the shear stress-shear displacement planes (Figs. 5a-7a), on the whole, all samples
207 firstly experience the elastic-perfectly and the plastic deformation procedures, until
208 reaching a peak shear stress at about 1.5 mm shear displacement. Then, the stress curves
209 follow the stress softening process, till a relatively stable shear stress is produced
210 beyond about 6 mm shear displacement. On the other hand, it appears that the stress-
211 displacement curve for $C_u = 1.85$ lies the highest under a given normal stress (Figs. 5a-
212 7a). As C_u increases, the peak shear stress presents lower values. Moreover, this
213 difference seems to be more significant as the normal stress increases.

214 For the relationship between the vertical displacement and the shear displacement,
215 all samples present negligible contraction followed by dilatancy (Figs. 5b-7b). With a
216 lower value of C_u, larger vertical displacement can be identified under a given normal
217 stress and a given shear displacement. This indicates the more pronounced dilatative
218 behavior during the shearing process for the soil sample with lower C_u values.

219 ***Variations of Friction Angle and Maximum Vertical Displacement***

220 To have a better understanding of the effect of the grain size distribution of this sandy
221 soil on the soil-structure interface behaviors, the friction angle φ at the soil-structure
222 interface and the maximum vertical displacement $d_{v-\max}$ are compared for each sample.
223 Fig. 8 shows the definition of the friction angle φ for the soil-structure interface (the
224 peak/maximum shear stress of S1 sample is taken as an example). Note that for the soil-
225 structure interface shear test, especially for the cohesionless soil (like sand used in this
226 study), the fitting between the interface shear stress and the normal stress can be
227 considered through the origin in the plot (see for examples in Hu and Pu 2004; Wang
228 et al. 2013; Eid et al. 2015). Thus, this fitting method is also applied for the
229 determinations of the interface friction angle in this study. Following this method, it can
230 be observed from Fig. 8 that the variation of the shear stress σ_s with the normal stress
231 σ_n presents a linear relationship with high accuracy (coefficient of determination
232 $R^2 = 0.990$), determining the tangent value of the friction angle ($\tan\varphi$) as the slope of
233 the fitting line. Table 2 lists the coefficients of determination R^2 for the friction angles
234 at peak and ultimate states for all samples. It can be seen that the R^2 values are no less
235 than 0.987, verifying the accuracies of the determinations of the interface friction angle
236 at both peak and ultimate states.

237 Fig. 9 depicts the variations of the friction angle for the soil-structure interface at
238 peak and ultimate states with the coefficient of uniformity C_u for each sample.
239 Distinct stress softening behavior is identified for a given sample during the shearing
240 process, with higher values of the friction angle at peak state than the ultimate state.
241 With C_u increasing, the friction angles at both peak and ultimate states decrease

linearly. In other words, for a structure surface with a given normalized roughness (with R_n higher than the critical value), the soil-structure interface provides a higher shearing resistance for the granular soils with a lower C_u value. Furthermore, the friction angle at peak state seems to decrease more rapidly than the ultimate state as C_u increases.

The variation of the maximum vertical displacement $d_{v-\max}$ against the coefficient of uniformity C_u is plotted in Fig. 10 for each sample under the three normal stresses. For a given sample, the maximum vertical displacement shows a higher value under a lower normal stress, suggesting that the soil sample presents the more significant dilative behavior under lower normal stresses. Under each normal stress, the linear relationship can be observed between the maximum vertical displacement and the coefficient of uniformity, with high fitting accuracies ($R^2 \geq 0.994$). As C_u increases, the maximum vertical displacement decreases, presenting the less pronounced dilative behavior of the sample. The less dilatancy or the less particle movement during the shearing process leads to the decrease of the shearing resistance at a higher C_u value accordingly, which is consistent with the testing results shown in Fig. 9. Furthermore, with the increase of the C_u value, the difference between the maximum vertical displacements of the sample under various normal stresses appears to decrease slightly.

Discussions

Interpretation of Interface Interactions

To interpret the mechanism of the variations of the friction angle with C_u, two extreme

264 cases are considered. Spheres are used to represent the granular soil particles in the
265 shear box. Fig. 11 and Table 3 show the details of the grain size distribution curves and
266 the mass fractions of these two cases, respectively. The maximum, the mean and the
267 minimum grain sizes of these two cases are kept the same as the present test (Fig. 11).
268 For Case I (nearly monodisperse material), the soil particles consist of 98% spheres
269 with diameter around 0.795 mm (d_{50}), showing the C_u value close to 1. However, for
270 Case II (nearly polydisperse material), the large (1.99 mm diameter) and the small (0.21
271 mm diameter) spheres both account for 49% of the mass of the material, determining
272 the C_u value close to 10. To investigate the sphere distributions in the shear box, the
273 PFC2D software was used to generate the soil samples randomly in a shear box (50 mm
274 length, 10 mm height) with the bottom as the regular saw-tooth plate ($R_{\max}$ = 0.636 mm,
275 R_n = 0.8). Note that due to the lack of parameters for the maximum and the minimum
276 dry densities for these two cases, the porosities of these two samples were both set at
277 0.36 as the value of S1 sample in the present test (Table 1).

278 Fig. 11 plots the generated soil samples in the shear box and the magnification of
279 two typical interface views of the two cases. For Case I ($C_u \approx 1$), the particles close to
280 the interface fall in the saw tooth, because of the smaller particle size than the size of
281 the saw tooth (Fig. 11a). These fallen particles are thus interlocked by the saw tooth.
282 Then, the other particles with similar diameter join tightly with the fallen particles to
283 form the main force chain during the shearing process.

284 For Case II ($C_u \approx 10$), the small particles (0.21 mm diameter) fall in the saw tooth.
285 With plenty of the fallen small particles, a new effective interface is generated (Su et al.

2018), as shown by the surface of the colored spheres in the magnification figures of Fig. 11b. Then, the interactions of other particles with this effective interface can be divided into two situations. Because of the small diameters of the particles forming the new effective interface, this newly generated surface roughness value [lower than the radius of the small particle (0.105 mm) for two horizontally abreast spheres] is much smaller than the roughness of the saw-tooth plate and the diameter of the coarse grains (1.99 mm). When the coarse grains (1.99 mm diameter) move along the effective interface (Fig. 11b), the R_n value is extremely low (for two horizontally abreast small spheres, $R_n < 0.105/1.99$). According to Jing et al. (2018) and Su et al. (2018), this interface can be considered as smooth, thus presenting negligible values of the interface friction angle. On the other hand, when the small particles contact with the effective interface, the main force chain is generated (Fig. 11b). As reported by several literatures, the contact force chain by smaller particles shows lower values of shearing resistance compared to that formed by larger particles (Wang et al. 2017, 2018b, 2018c). That is to say, in combination with the two aforementioned interactions in Case II, the shearing resistance mainly provided by the force chain of the smaller particles (0.21 mm diameter) in Case II is expected to show lower values than that formed by the larger particles (around 0.795 mm diameter) in Case I. This interpretation has a good agreement with the observations in the present tests: for a given condition, with the lower C_u value of the granular soil, the soil-structure interface provides the higher shearing resistance.

Comparison of Present and Previous Studies

To verify the observations in the present test, several relevant studies are chosen to be compared in terms of the friction angle at peak state. Table 4 lists the soil properties and the testing details of the present and previous studies. The friction angles at the peak state are plotted versus C_u for these studies in Fig. 12. The previous investigations about the effect of the grain size distribution of soils on the friction angle include not only the interface shear test, but also direct shear tests, consolidated drained/undrained triaxial tests and DEM (discrete element method) simulations (Table 4).

On the whole, the testing results of the friction angle all decrease with the increase of C_u, lying in a range defined by the upper and the lower bounds (Fig. 12). For the previous interface shear test (Liang et al. 2017), the decreasing rate of the friction angle with C_u is less significant than that in the present test. This is probably due to the different d_{50} values for each sample (Liang et al. 2017), leading to the variations of R_n and thus influencing the interface friction angle. For the other tests without the structure interface, the friction angle between soil particles also decreases as C_u increases, while the values of the friction angle and the variation rate are different for each study. This is because except for C_u, the shearing behavior of soils is also affected by the soil type, the maximum, the mean and the minimum grain sizes, the relative density, the water content, etc. The comparison between the present and previous studies in Fig. 12 is an overall analysis of the existing data for both the soil materials and the soil-structure interface. In summary, the previous studies still provide a strong support for the variations of the friction angle with C_u identified in the present study.

Limitations of this Study

It is important to mention that the present and the existing relevant studies are all focused on the granular soils, such as sands and gravels with low or negligible plasticity. The plasticity effect is not considered for the sandy soil (or granular soil) in this study. Thus, the identified observations are suitable for these granular materials, with the other influencing factors kept the same (only the grain size distribution is considered as the variable). However, for the soils with high plasticity (such as clay or silt), the decreasing trend of the shearing resistance with the coefficient of uniformity might be different due to the extra contribution of the cohesion, which cannot be negligible for these soils. To clarify this issue related to the soils with high plasticity, more studies are needed.

Note also that normalized surface roughness R_n is selected at a value (0.8 in this study) higher than the critical value (around 0.4) identified by Su et al. (2018) for the same kind of sand, to ensure the stable state of the interface friction angle. At this state, the interface friction angle keeps constant, regardless of the changes of R_n. Hence, the present observations and interpretations are available for the soil-structure interface when the normalized surface roughness exceeds the critical value.

Conclusions

This study investigates the effect of the grain size distribution of a sandy soil on the shearing behaviors at the soil-structure interface using a modified direct shear apparatus. The testing accuracy of the present testing method was firstly verified by repeatability tests using three S1 samples ($C_u = 1.85$) under 50 kPa normal stress. Appropriate

352 consistency of the testing results was obtained for these three samples, ensuring the
353 accuracy of the following tests. Five samples with different grain size distribution
354 curves were prepared. During sample preparation, the maximum, the mean and the
355 minimum grain sizes, the relative density and the normalized roughness of the interface
356 were all kept the same for each sample. The variations of the friction angle for the soil-
357 structure interface and the maximum vertical displacement with the coefficient of
358 uniformity C_u were analyzed.

359 With a lower C_u, the shear stress curve lies higher in the shear stress-shear
360 displacement plane under a given normal stress. As C_u increases, the friction angle
361 for the soil-structure interface decreases at both peak and ultimate states, with a higher
362 decreasing rate for the peak state. For a given sample, the maximum vertical
363 displacement shows higher values under lower normal stresses, suggesting the more
364 dilative behavior. With C_u increasing under a given normal stress, less dilatancy or
365 less particle movement is identified during the shearing process, thus presenting a lower
366 shearing resistance.

367 The experimental observations are interpreted from the micro-mechanism of the
368 particle contact. For the granular sample with an extremely low C_u value (≈ 1), the
369 shearing behavior is dominated by the contacts between coarser grains (diameter around
370 0.795 mm in this study). However, for the granular sample with an extremely high C_u
371 value (≈ 10), the contacts between finer grains (diameter around 0.212 mm in this study)
372 form the main force chain, thus leading to a lower shearing resistance. In comparison
373 with the previous relevant studies, the observations about the decreasing trend of the

374 friction angle (at peak state) with the increase of C_u are also strongly verified.

375

376 **Acknowledgement**

377 The present work was carried out with the support of the Science and Technology
378 Development Fund, Macao S.A.R (FDCT, Code 193/2017/A3), the National Natural
379 Science Foundation of China (Grant No. 51508585), and the University of Macau
380 Research Fund (MYRG2017-00198-FST).

381

382 **Notation**

383 *The following symbols are used in this paper:*

A = particle image projection area

C_u = uniformity of coefficient

d_{50} = mean grain size

$d_{\max}$ = maximum grain size

$d_{\min}$ = minimum grain size

d_s = specific gravity

$d_{v-\max}$ = maximum vertical displacement

D_d = relative density

n = porosity

P = particle image projection perimeter

$R_{\max}$ = maximum surface roughness

R_n = normalized surface roughness

R^2 = coefficient of determination

ρ_d = dry density

$\rho_{d\max}$ = maximum dry density

$\rho_{d\min}$ = minimum dry density

σ_n = normal stress

σ_s = shear stress

φ = friction angle

π = circular constant

References

Abu-Farsakh, M., Coronel, J., and Tao, M. 2007. "Effect of soil moisture content and dry density on cohesive soil–geosynthetic interactions using large direct shear tests." *J. Mater. Civ. Eng.*, 19 (7): 540-549.

Anubhav, and Basudhar, P. K. 2013. "Interface behavior of woven geotextile with rounded and angular particle sand." *J. Mater. Civ. Eng.*, 25 (12): 1970-1974.

Arulrajah, A., Rahman, M. A., Piratheepan, J., Bo, M. W., and Imteaz, M. A. 2014. "Evaluation of interface shear strength properties of geogrid-reinforced construction and demolition materials using a modified large-scale direct shear testing apparatus." *J. Mater. Civ. Eng.* 26 (5): 974-982.

ASTM. (2011). "Standard test method for direct shear test of soils under consolidated drained conditions." ASTM D3080, West Conshohocken, PA: USA.

ASTM. 2016a. "Standard test methods for maximum index density and unit weight of

soils using a vibratory table." ASTM D4253, West Conshohocken, PA: ASTM.

ASTM. 2016b. "Standard test methods for minimum index density and unit weight of soils and calculation of relative density." ASTM D4254, West Conshohocken, PA: ASTM.

ASTM. 2017. "Standard practice for classification of soils for engineering purposes (unified soil classification system)." ASTM D2487, West Conshohocken, PA: ASTM.

Chen, Q., Abu-Farsakh, M., Voyiadjis, G. Z., and Souci, G. 2013. "Shakedown analysis of geogrid-reinforced granular base material." *J. Mater. Civ. Eng.*, 25 (3): 337-346.

Chen, X., Zhang, J., Xiao, Y., and Li, J. 2015. "Effect of roughness on shear behavior of red clay–concrete interface in large-scale direct shear tests." *Can. Geotech. J.* 52 (8): 1122-1135.

DeJong, H. T., and Westgate, Z. J. 2009. "Role of initial state, material properties, and confinement condition on local and global soil-structure interface behavior." *J. Geotech. Geoenviron. Eng.* 135 (11): 1646-1660.

Desai, C. S., Drumm, E. C., and Zaman, M. M. 1985. "Cyclic testing and modeling of interfaces." *J. Geotech. Eng.* 111 (6): 793–815.

Divya, P. V., Viswanadham, B. V. S., and Gourc, J. P. 2014. "Evaluation of tensile strength-strain characteristics of fiber-reinforced soil through laboratory tests." *J. Mater. Civ. Eng.* 26 (1): 14-23.

Dove, J. E., and Jarrett, J. B. 2002. "Behavior of dilative sand interfaces in a geotribology framework." *J. Geotech. Geoenviron. Eng.* 128 (1): 25-37.

Eid, H. T., Amarasinghe, R. S., Rabie, K. H., and Wijewickreme, D. 2015. "Residual shear strength of fine-grained soils and soil–solid interfaces at low effective normal stresses." *Can. Geotech. J.* 52 (2): 198-210.

Fatahi, B., Nguyen, Q. V., Xu, R., and Sun, W. J. 2018. "Three-dimensional response of neighboring buildings sitting on pile foundations to seismic pounding." *Int. J. Geomech.* 18 (4): 04018007.

Goodarzi, S., and Shahnazari, S. 2019. "Strength enhancement of geotextile-reinforced carbonate sand." *Geotext. Geomem.* 47: 128-139.

Hamid, T. B., and Miller, G. A. 2009. "Shear strength of unsaturated soil interfaces." *Can. Geotech. J.* 46: 595–606.

Hentschel, M. L., and Page, N. W. 2003. "Selection of descriptors for particle shape characterization." *Part. Part. Syst. Charact.* 20: 25-38.

Hokmabadi, A. S., Fatahi, B., and Samali, B. 2014. "Assessment of soil–pile–structure interaction influencing seismic response of mid-rise buildings sitting on floating pile foundations." Comput. Geotech. 55: 172-186.

Hokmabadi, A. S., Fatahi, B., and Samali, B. 2015. "Physical modeling of seismic soil-pile-structure interaction for buildings on soft soils." *Int. J. Geomech.* 15 (2): 04014046.

Hu, L., and Pu, J., 2004. "Testing and modeling of soil-structure interface." *J. Geotech. Geoenviron. Eng.* 130 (8): 851-860.

Jensen, R. P., Bosscher, P. J., Plesha, M. E., and Edil, T. B. 1999. "DEM simulation of granular media-structure interface: effects of surface roughness and particle shape."

442 *Int. J. Numer. Anal. Met. Geomech.* 23: 531–547.
443 Jing, X. Y., Zhou, W. H., Zhu, H. X., Yin, Z. Y., and Li, Y. 2018. "Analysis of soil-
444 structural interface behavior using three- dimensional DEM simulations." *Int. J.*
445 *Numer. Anal. Met. Geomech.* 42 (2): 339-357.
446 Karimi, Z., and Dashti, S. 2016. "Numerical and centrifuge modeling of seismic soil–
447 foundation–structure interaction on liquefiable ground." *J. Geotech. Geoenviron.*
448 *Eng.* 142 (1): 04015061.
449 Kokusho, T., Hara, T., and Hiraoka, R. 2004. "Undrained shear strength of granular
450 soils with different particle gradations." *J. Geotech. Geoenviron. Eng.* 130 (6):
451 621–629.
452 Li, S., Zhou, W. H., Jing, X. Y., and Zhu, H. X. 2018. "Evaluation of grain shape
453 parameters of Fujian standard sand." In *China-Europe Conference on Geotechnical*
454 *Engineering*. Vienna, Austria: Springer Series in Geomechanics and
455 Geoengineering.
456 Liang, Y., Yeh, T. C. J., Wang, J., Liu, M., and Hao, Y. 2017. "Effect of particle size
457 distribution on soil-steel interface shear behavior." *Soil Mech. Found. Eng.* 54 (5):
458 310-317.
459 Liu, Y., Li, G., Yin, Z., Dano, C., Hicher, P. Y., Wang, J. H., and Xia, X. H. 2014.
460 "Influence of grading on undrained behavior of granular materials." *Comptes*
461 *Rendus Mécanique* 342 (2): 85-95.
462 Mortara, G., Mangiola, A., and Ghionna, V. N. 2007. "Cyclic shear stress degradation
463 and post-cyclic behaviour from sand–steel interface direct shear tests." *Can.*

464 *Geotech. J.* 44 (7): 739-752.
465 Nguyen, Q. V., Fatahi, B., and Hokmabadi, A. S. 2017. "Influence of size and load-
466 bearing mechanism of piles on seismic performance of buildings considering soil-
467 pile-structure interaction." *Int. J. Geomech.* 17 (7): 04017007.
468 Norsyahariati, N. D. N., Hui, K. R., and Juliana, A. G. A. 2016. "The effect of soil
469 particle arrangement on shear strength behavior of silty sand." In *3rd Int. Conf. on*
470 *Civil and Environmental Engineering for Sustainability*, 47, 03022. Melaka,
471 Malaysia: MATEC Web of Conferences.
472 Oumarou, T. A., and Evgin, E. 2005. "Cyclic behaviour of a sand – steel plate interface."
473 *Can. Geotech. J.* 42: 1695–1704.
474 Qian, Y., Han, J., Pokharel, S. K., and Parsons, R. L. 2013. "Performance of triangular
475 aperture geogrid-reinforced base courses over weak subgrade under cyclic loading."
476 *J. Mater. Civ. Eng.*, 25 (8): 1013-1021.
477 Seif El Dine, B., Dupla, J. C., Frank, R., Canou, J., and Kazan, Y. 2010. "Mechanical
478 characterization of matrix coarse-grained soils with a large-sized triaxial device."
479 *Can. Geotech. J.* 47 (4): 425–438.
480 Su, L. J., Zhou, W. H., Chen W. B. and Jie X. X. (2018). "Effects of relative roughness
481 and mean particle size on the shear strength of sand-steel interface." *Measurement*
482 122: 339-346.
483 Tabatabaiefar, S. H. R., Fatahi, B., and Samali, B. 2013. "Seismic behavior of building
484 frames considering dynamic soil-structure interaction." *Int. J. Geomech.* 13 (4):
485 409-420.

Trombetta, N. W., Mason, H. B., Hutchinson, T. C., Zupan, J. B., Bray, J. D., Kutter, B. L. 2014. "Nonlinear soil-foundation-structure and structure-soil-structure interaction: Centrifuge test observations." *J. Geotech. Geoenviron. Eng.* 140 (5): 04013057.

Turan, A., Hinchberger, S. D., and El Naggar, M. H. 2013. "Seismic soil–structure interaction in buildings on stiff clay with embedded basement stories." *Can. Geotech. J.* 50: 858–873.

Uesugi, M., and Kishida, H. 1986. "Frictional resistance at yield between dry sand and mild steel." *Soils Found.* 26 (4):139- 149.

Venkateswarlu, H., Ujjawal, K. N., and Hegde, A. 2018. "Laboratory and numerical investigation of machine foundations reinforced with geogrids and geocells." *Geotext. Geomem.* 46: 882-896.

Wang, H. L., Cui, Y. J., Lamas-Lopez, F., Dupla, J. C., Canou, J., Calon, N., Saussine, G., Aimedieu, P., and Chen, R. P. 2017. "Effects of inclusion contents on resilient modulus and damping ratio of unsaturated track-bed materials." *Can. Geotech. J.* 54: 1672-1681.

Wang, H. L., Chen, R. P., Qi, S., Cheng, W., and Cui, Y. J. 2018a. "Long-term performance of pile-supported ballastless track-bed at various water levels." *J. Geotech. Geoenviron. Eng.* 144 (6): 04018035.

Wang, H. L., Cui, Y. J., Lamas-Lopez, F., Dupla, J. C., Canou, J., Calon, N., Saussine, G., Aimedieu, P., and Chen, R. P. 2018b. "Investigation on the mechanical behavior of track-bed materials at various contents of coarse grains." *Constr. Build. Mater.*

164: 228-237.

Wang, H. L., Cui, Y. J., Lamas-Lopez, F., Dupla, J. C., Canou, J., Calon, N., Saussine, G., Aimedieu, P., and Chen, R. P. 2018c. "Permanent deformation of track-bed materials at various inclusion contents under large number of loading cycles." *J. Geotech. Geoenviron. Eng.* 144 (8): 04018044.

Wang, H. L., and Chen, R. P., 2019. "Estimating static and dynamic stresses in geosynthetic-reinforced pile-supported track-bed under train moving loads." *J. Geotech. Geoenviron. Eng.* in press. doi: 10.1061/(ASCE)GT.1943-5606.0002056.

Wang, H. L., Chen, R. P., Cheng, W., Qi, S., and Cui, Y. J. 2019a. "Full-scale model study on variations of soil stress in geosynthetic-reinforced pile-supported track-bed with water level change and cyclic loading". *Can. Geotech. J.* 56(1): 60–68.

Wang, H. L., Chen, R. P., Liu, Q. W., and Kang, X. 2019b. "Investigation on geogrid reinforcement and pile efficacy in geosynthetic-reinforced pile-supported track-bed." *Geotext. Geomem.* in press.

Wang, H. L., Chen, R. P., Liu, Q. W., Kang, X., and Wang, Y. W. 2019c. "Soil-geogrid interaction at various influencing factors by pullout tests with applications of FBG sensors." *J. Mat. Civil Eng.* 31 (1): 04018342.

Wang, J. J., Zhang, H. P., Tang, S. C., and Liang, Y. 2013. "Effects of particle size distribution on shear strength of accumulation soil." *J. Geotech. Geoenviron. Eng.* 139 (11): 1994–1997.

Wichtmann, T., and Triantafyllidis, T. 2009. "Influence of the grain-size distribution curve of quartz sand on the small strain shear modulus Gmax." *J. Geotech.*

530 *Geoenviron. Eng.* 135 (10), 1404–1418.

531 Wichtmann, T., and Triantafyllidis, T. 2013. "Effect of uniformity coefficient on
532 G/Gmax and damping ratio of uniform to well-graded quartz sands." *J. Geotech.*
533 *Geoenviron. Eng.* 139 (1): 59-72.

534 Yan, W. M., and Dong, J. 2011. "Effect of particle grading on the response of an
535 idealized granular assemblage." *Int. J. Geomech.* 11 (4): 276-285.

536 Yin J. H. and Zhou W. H. 2009. "Influence of grouting pressure and overburden stress
537 on the interface resistance of a soil nail." *J. Geotech. Geoenviron. Eng.* 135 (9):
538 1198-1208.

539 Zeghal, M., and Edil, T.B. 2002. "Soil structure interaction analysis: modeling the
540 interface." *Can. Geotech. J.* 39 (3): 620–628.

541 Zhang, G., and Zhang, J. 2006. "Monotonic and cyclic tests of interface between
542 structure and gravelly soil." *Soils Found.* 46 (4): 505–518.

543 Zhou W. H., and Yin J. H. 2008. "A simple mathematical model for soil nail and soil
544 interaction analysis." *Comput. Geotech.* 35 (3): 479-488.

545 Zhou, W. H., Jing, X. Y., and Yin, Z. Y. 2019. "Effects of particle sphericity and initial
546 fabric on the shearing behavior of soil-rough structural interface." *Acta Geotech*.
547 in press. doi: 10.1007/s11440-019-00781-2.

548 Zhou, W. H., Yin, J. H., and Hong, C.Y. 2011. "Finite element modelling of pullout
549 testing on a soil nail in a pullout box under different overburden and grouting
550 pressures." *Can. Geotech. J.* 48 (4): 557-567.

551 Zhou, W. H., Yuen, K. V., and Tan, F. 2013. "Estimation of maximum pullout shear

552 stress of grouted soil nails using Bayesian probabilistic approach.” *Int. J. Geomech.*
553 13 (5): 659–664.
554 Zhu, H., Zhou, W. H., and Yin, Z. Y. 2018. “Deformation mechanism of strain
555 localization in 2D numerical interface tests.” *Acta Geotech.* 13 (3): 557-573.

Table 1. Soil properties

Sample	d_{50} (mm)	C_u	ρ_{dmax} (g/cm^3)	ρ_{dmin} (g/cm^3)	D_d (%)	d_s	n
S1	0.795	1.85	1.720	1.580	90	2.67	0.36
S2	0.795	2.81	1.830	1.700	90	2.67	0.32
S3	0.795	3.75	1.850	1.710	90	2.67	0.31
S4	0.795	4.67	1.870	1.710	90	2.67	0.31
S5	0.795	5.20	1.890	1.690	90	2.67	0.30

Note: d_{50} = mean grain size; C_u = coefficient of uniformity; ρ_{dmax} = maximum dry density (ASTM 2016a); ρ_{dmin} = minimum dry density (ASTM 2016b); D_d = relative density, which can be expressed as $D_d = \frac{\rho_{d\max}(\rho_d - \rho_{d\min})}{\rho_d(\rho_{d\max} - \rho_{d\min})} \times 100$ (ASTM 2016a, 2016b); ρ_d = dry density; d_s = specific gravity; n = porosity.

Table 2. Coefficients of determination R^2 for the friction angles at peak and ultimate state

Sample	S1	S2	S3	S4	S5
Peak	0.990	0.993	0.987	0.997	0.998
Ultimate	0.990	0.998	0.993	0.999	0.990

Table 3. Material properties of the two extreme cases

Sphere diameter (mm)	Mass fraction (%)	
	Case I	Case II
1.99	1	49
0.8	49	1
0.79	49	1
0.21	1	49
C_u	≈ 1	≈ 10

Table 4. Soil properties and testing setups

Studies	Material	d_{50} (mm)	d_{max} (mm)	d_{min} (mm)	C_u	D_d (%)	Testing type
Present test	Sand	0.795	2	0.212	1.85-5.20	90	IS
Liang et al. (2017)	Sand-stone	0.17-1.06	2	0.07	2.4-7.2	NA	IS
Norsyahariati et al. (2016) [1]	Silty sand	NA	NA	NA	2-3.4	NA	DS
Liu et al. (2014) [2]	Sand	0.9	1.6 -2	0.08-0.48	1.1-20	41.3-42.9	CU
Liu et al. (2014) [2]	Glass ball	0.9	1.6-2	0.08-0.48	1.1-20	41.4-43.1	CU
Wang et al. (2013)	Sand-rock	1.1-7.1	10	0.07	2.2-17.6	NA	T
Yan and Dong (2011) [3]	Sphere	2.4	6	0.2	1-2.17	NA	CD

Note: d_{50} = mean grain size; d_{max} = maximum grain size; d_{min} = minimum grain size; C_u = coefficient of uniformity; D_d = relative density; IS = interface shear test; NA = not applicable; DS = direct shear test; CU = consolidated undrained triaxial test; T = triaxial test; CD = consolidated drained triaxial test.

[1] The liquid limit and the plasticity index of fines (particle size < 0.075 mm) in the soils are 24.4-25.32 and 0.44-0.54, respectively.

[2] The friction angle of total stress is used in Fig. 12.

[3] This study is based on DEM (discrete element method) simulation.

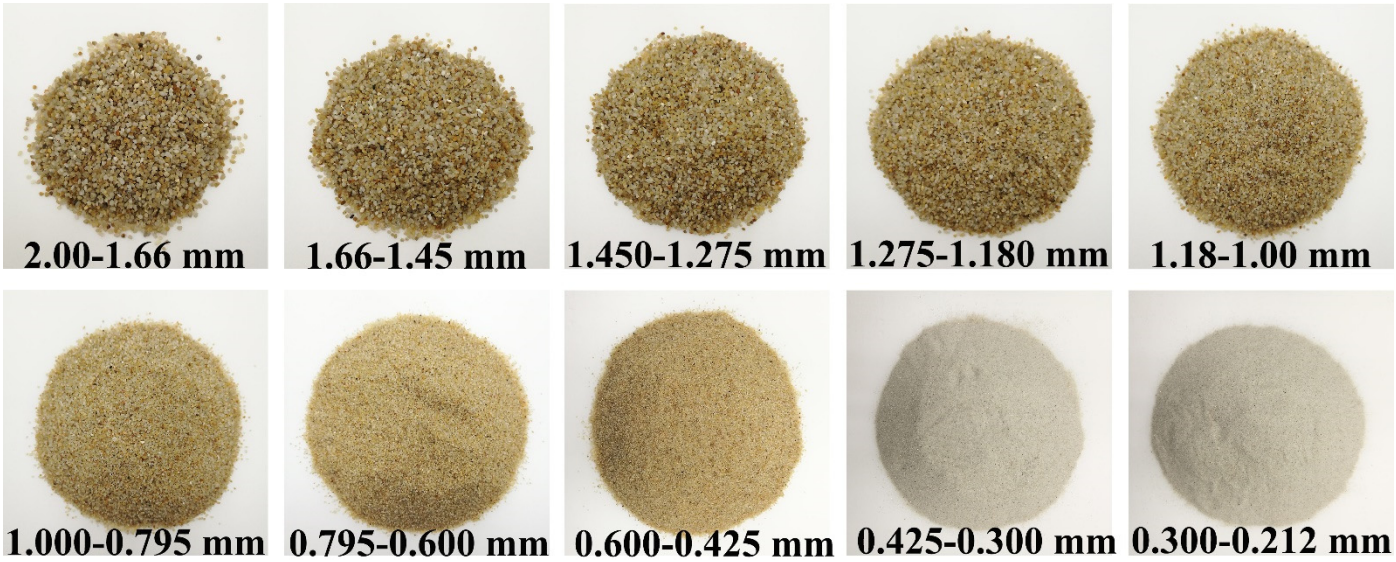

Fig. 1. Photo views of the sand particles (100 g mass for each photo) at different ranges of grain sizes

Note: for each photo, the soil particles represent those passing the sieve with the larger size and retaining on the sieve with the smaller size.

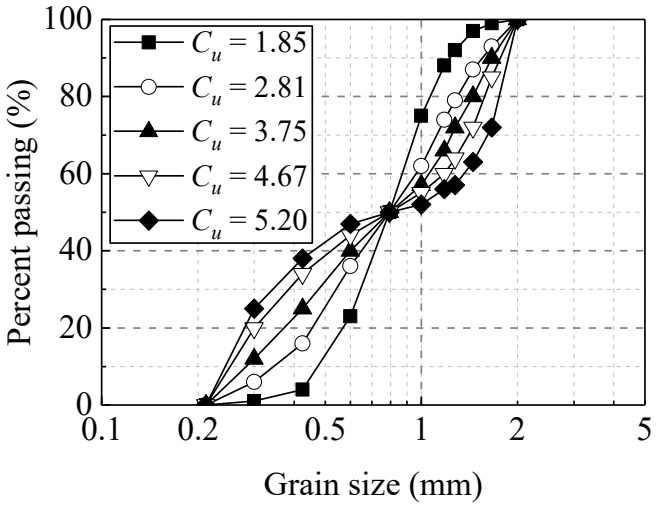

Fig. 2. Grain size distributions of the testing soils (logarithmic horizontal axis)

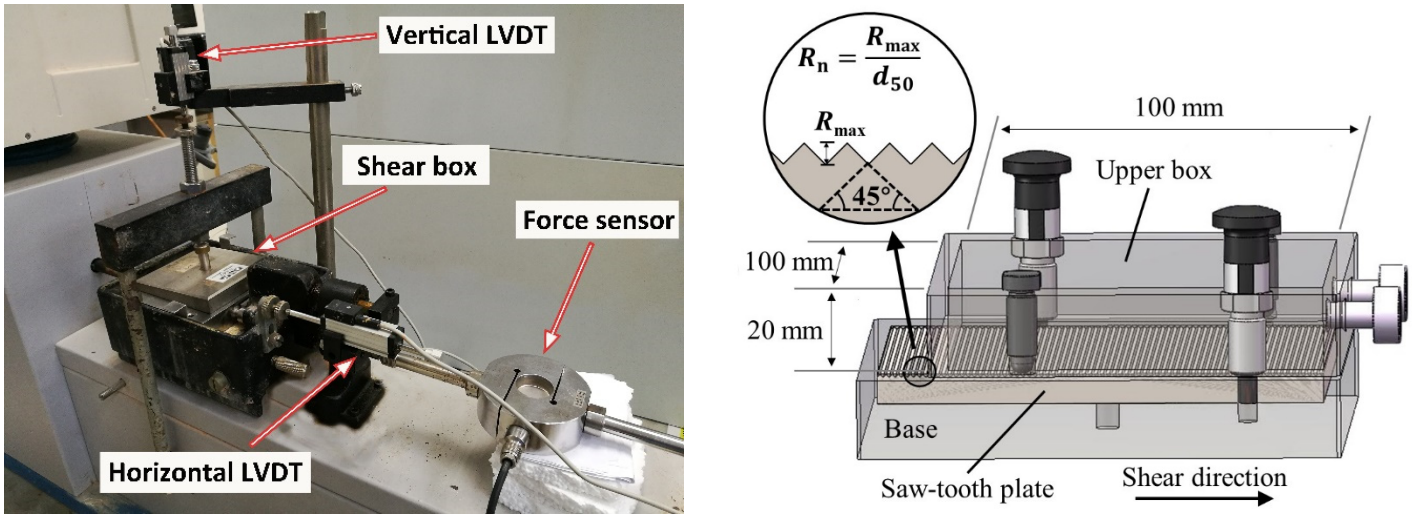

(a) (b)

Fig. 3. Schematic view of (a) the modified direct shear apparatus and (b) the shear box

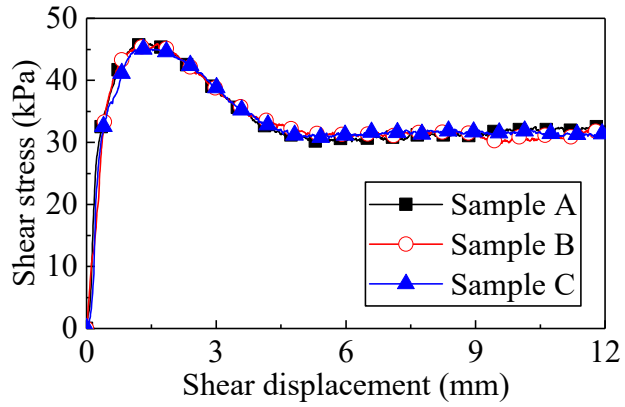

(a)

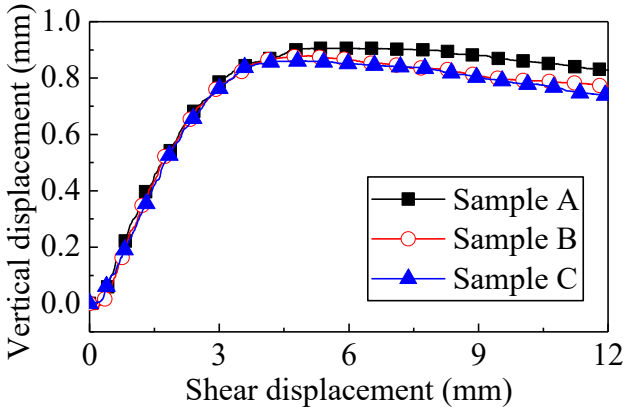

(b)

Fig. 4. Repeatability testing results: variations of (a) shear stress and (b) vertical displacement with shear displacement for three S1 samples under 50 kPa normal stress

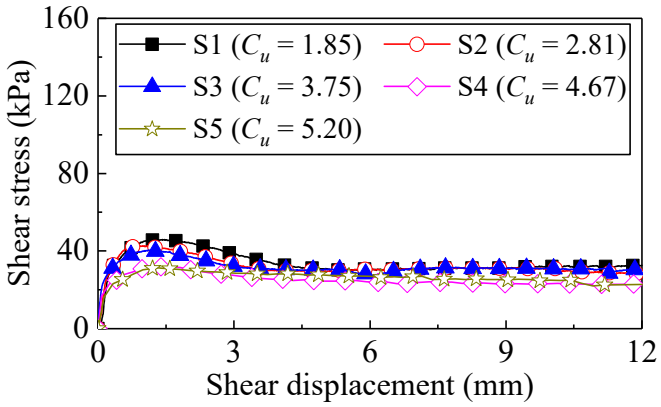

(a)

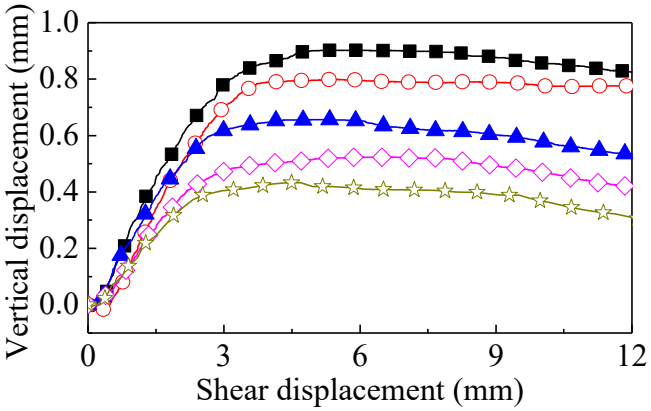

(b)

Fig. 5. Variations of (a) shear stress and (b) vertical displacement with shear displacement under 50 kPa normal stress

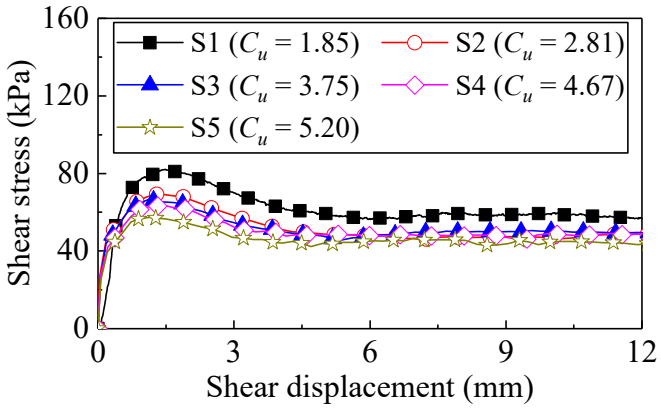

(a)

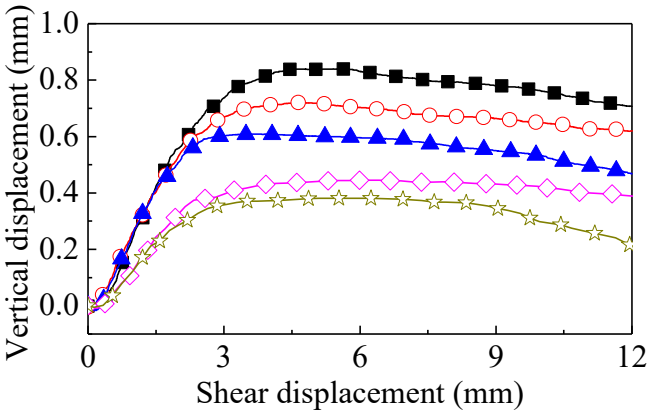

(b)

Fig. 6. Variations of (a) shear stress and (b) vertical displacement with shear displacement under 100 kPa normal stress

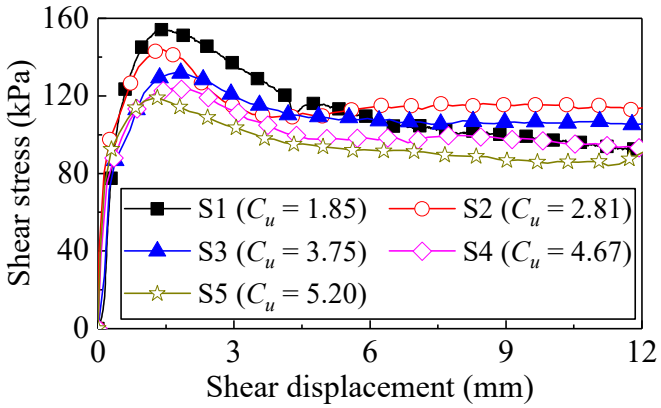

(a)

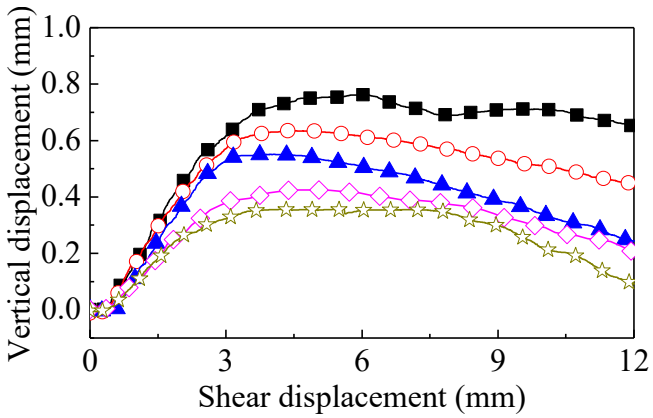

(b)

Fig. 7. Variations of (a) shear stress and (b) vertical displacement with shear displacement under 200 kPa normal stress

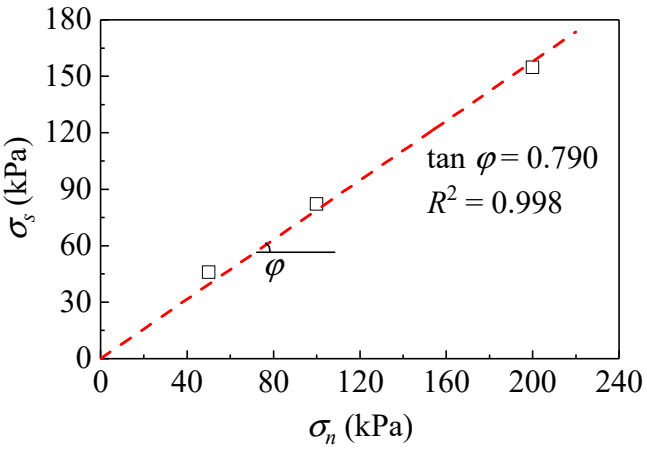

Fig. 8. Determination of friction angle for the soil-structure interface (for sample S1 at peak state)

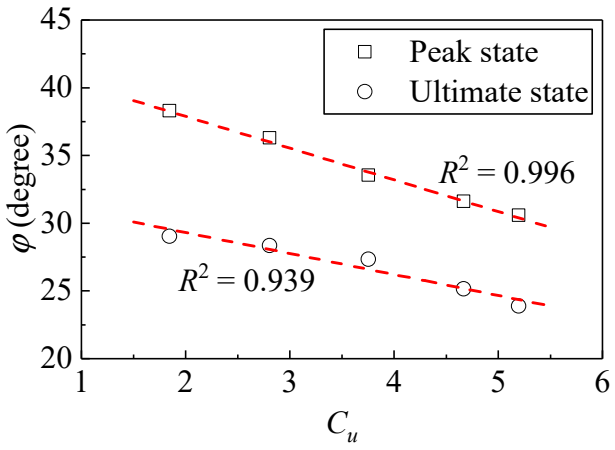

Fig. 9. Variations of friction angle for the soil-structure interface at peak and ultimate states with C_u

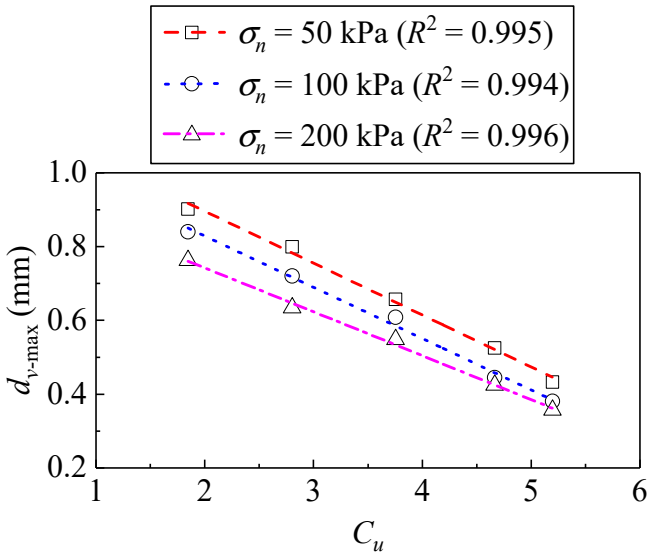

Fig. 10. Variations of maximum vertical displacement with C_u

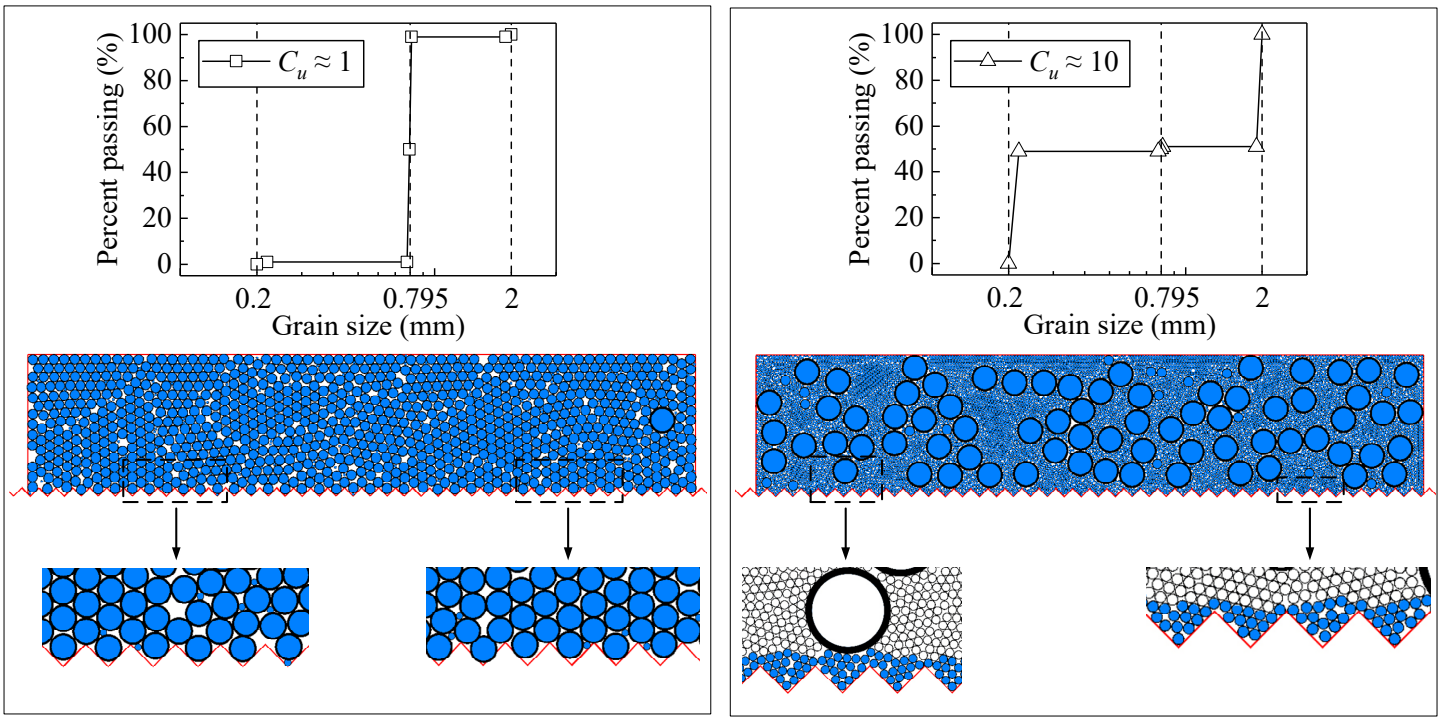

(a) (b)

Fig. 11. Interpretation of interface interactions: (a) $C_u \approx 1$; (b) $C_u \approx 10$

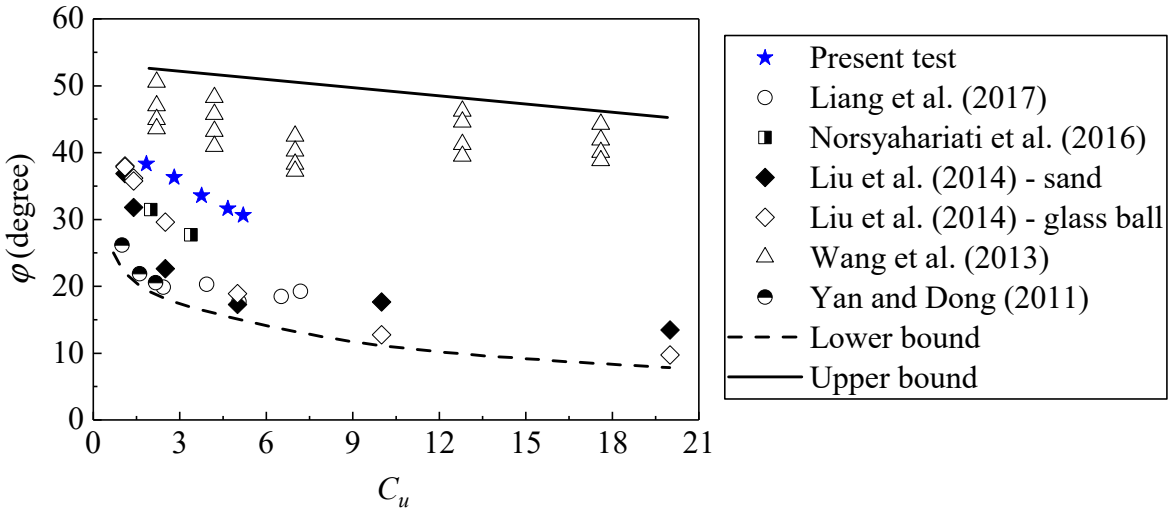

Fig. 12. Comparisons of friction angle at peak state between the present test and the literatures